Bubble Dynamics During Degassing of Liquids at Microgravity Conditions

Nikolaos Divinis
Dept. of Chemistry, Aristotle University, Univ. Box 116, 541 24 Thessaloniki, Greece; and Dept. of Mechanical Engineering, University of Thessaly, Pedion Areos, 38 334 Volos, Greece

Thodoris D. Karapantsios
Dept. of Chemistry, Aristotle University, Univ. Box 116, 541 24 Thessaloniki, Greece

Robert de Bruijn
Van der Waals-Zeeman Instituut, Universiteit van Amsterdam, Valckenierstraat 65, 1018 XE Amsterdam, The Netherlands

Margaritis Kostoglou
Dept. of Chemistry, Aristotle University, Univ. Box 116, 541 24 Thessaloniki, Greece

Vasilis Bontozoglou
Dept. of Mechanical Engineering, University of Thessaly, Pedion Areos, 38 334 Volos, Greece

Jean-Claude Legros
Universite Libre de Bruxelles, Service de chimie-physique E.P. CP 165, 50 Ave F.D. Roosevelt, B-1050 Brussels, Belgium

DOI 10.1002/aic.10926
Published online July 13, 2006 in Wiley InterScience (www.interscience.wiley.com).

This work investigates the growth of bubbles generated in a liquid saturated with dissolved CO_2 when its temperature is rapidly and locally raised above the saturation value, still below the boiling point of the test liquid. Three test liquids with different physical and transport properties were studied: water, glycerine/water mixture 42/58 w/w, and n-heptane. Bubbles grow at the tip of a roughly spherical miniature heater (thermistor), whose temperature varies linearly with the power of an applied heat pulse. Nucleation and growth of single bubbles is studied, triggered either by continuous heat pulses or by intermittent heat pulses. A one-dimensional spherically symmetric bubble growth model based on heat and mass transfer on the liquid side is employed to extract the average bubble temperature evolution curves from the experimental bubble growth curves. Comparisons between extracted average bubble temperature evolution data and measured thermistor temperatures reveal features of the heat-triggered bubble growth.
 AIChE J, 52: 3029–3040, 2006
Keywords: bubble growth, diffusion, heat transfer, mass transfer, carbonated liquids

Introduction

The study of bubble generation and dynamics is important in industrial applications such as heat pumps, heat exchangers, cooling systems, microprocessor cooling, and material processing.[1-6] It is also of great significance in geology during the explosive degassing of magma encountered in volcanoes (for example, the eruption of Lake Nyos in Cameroon[7]). Bubble generation and growth dynamics is important also in food technology (for example, manufacturing of carbonated beverages or wine[8]) and in human physiology, where nitrogen bubbles can grow in the circulatory system of divers, astronauts, or

Correspondence concerning this article should be addressed to T. D. Karapantsios at karapant@chem.auth.gr.

even airplane passengers during serious decompression incidents[9-11] Finally, bubble generation and dynamics is important in studying physical phenomena such as nucleation and boiling.

In general, bubble growth and evolution is a complex process, involving nucleation as the first step and a combination of mass and/or heat and momentum transfer between the expanding bubble and the liquid during the subsequent growth.

There are many studies investigating heterogeneous nucleation on solid walls, either regarding boiling (vapor) bubbles or dissolved gas bubbles produced by a global reduction of pressure or increase of temperature in liquids[12-15] Other studies investigate the growth rate of bubbles controlled by mass transfer (such as dissolved gas bubbles[3]) or controlled by heat transfer (such as vapor bubbles[16]). There is also some work on comparable heat and mass transfer control during vapor bubble growth from a binary solution with a non-volatile solute.[17]

The governing relationships that describe the spherical symmetric bubble growth controlled by heat and mass transfer were formally introduced by Scriven.[18] Scriven presented a self-similar analytical solution for bubble growth in an infinite liquid of constant supersaturation, consisting of a parabolic law ($R \approx t^a$ with $a = 0.5$) for the temporal variation of the radius, R, of the bubble.

In boiling experiments, the reported values of the exponent a vary. Saddy and Jameson[19] proposed $a = 0.75$ for nucleate boiling of water. Strenge et al.[20] reported a values varying between 0.312 and 0.512 for pentane boiling. Furthermore, Rosner and Epstein[21] calculated deviations from the parabolic law for bubbles growing in a submicroscopic scale.

On the contrary, experiments on quasi-isothermal dissolved gas bubble growth from supersaturated solutions[8,14,22] consistently follow the parabolic law, from the inception of the gas bubble to the end of the growth period. It must be stressed, though, that these experiments were performed having in mind more the mechanism of nucleation rather than bubble growth.[15] This is the reason why most of those experiments were conducted at low temperatures where the effect of the liquid vapor pressure is insignificant.

The scope of the present work is to study bubble growth of a dissolved gas under conditions where both mass and heat diffusion but also liquid vapor pressure are significant. A small-size roughly spherical thermistor is used as a heater, in order to create local supersaturation in a large pool of saturated solution. In due course of time—varying according to the conditions of each run—bubble nucleation occurs, leading to concentration gradients that sustain the further growth of the bubble. Results from experiments with a flat plate heater geometry will be presented in a subsequent publication. Experiments are conducted at low gravity conditions in order to: (1) allow bubbles to grow up to large sizes without departing from the heater surface and , therefore, from the field of view of the camera; (2) avoid bubble distortion from sphericity; and (3) suppress natural convection of liquid thermal layers.

Because of the complexity of the phenomena taking place during bubble growth, a direct simulation of the problem is not possible at present. Instead, a simple one-dimensional (spherically symmetric) bubble growth model is used to extract the average bubble temperature evolution curves from the experimental bubble growth versus time curves. The model is based on momentum, heat, and mass transfer considerations on the liquid layer surrounding the expanding bubble surface. An effort is made to appraise the several phenomena that may govern bubble growth (such as mass diffusion induced gas desorption, evaporation, and Marangoni convection) from comparisons of the estimated average bubble temperature evolution curves with the experimentally obtained temperature evolution curves of the heating thermistor.

The outline of the work is as follows: First, a model for spherically symmetric non-isothermal bubble growth is developed. This is used to transform the bubble radius evolution curves into average bubble temperature evolution curves (solution of the inverse problem). The main experimental set-up and procedures used in the two ESA's (European Space Agency) parabolic flight campaigns is presented next. The experimental information involves temperature data and bubble growth data versus time for various liquids and heat powers. Finally, the experimental results are compared against the theoretical predictions in order to attempt an interpretation of the observed phenomena. This work is a follow-up of a previous investigation by Divinis et al.[23]

Theory

Motivation of the approach

The sequence of phenomena after the onset of the thermistor heating is the following: Initially, a transient temperature field develops in the liquid around the thermistor. As heat penetrates into the liquid, the thermistor surface temperature rapidly increases but gradually tends to level-off at a steady temperature where the heat delivered to the thermistor is fully removed by the liquid. At some moment—before or after reaching this steady temperature—supersaturation of dissolved CO_2 leads to the generation of a bubble on the thermistor's surface. This occurs at a high energy surface nucleation site (heterogeneous nucleation). The sudden burst of a bubble breaks the spherical symmetry of the temperature field imposed by the thermistor and renders the problem inherently three-dimensional.

A detailed mathematical description of the process includes the solution of transient heat and mass transfer equations in the gas and liquid phases along with the appropriate boundary conditions on the surface of the bubble and the thermistor. These equations are of the convection-diffusion type, where the flow field responsible for the convection terms is generated from the expanding bubble. Evidently, the problem includes a moving boundary, with the motion being part of the solution. In addition, the temperature gradient along the surface of the bubble induces a Marangoni motion, which transfers hot fluid from the thermistor to the remote parts of the bubble surface, tending to equilibrate bubble and thermistor temperatures. Although the complete problem can be easily formulated, its solution is not possible with present-day computer resources. Problems like the inherent three-dimensionality, the moving gas-liquid interface, and the inclusion of Marangoni effects could, in principle, be handled using advanced CFD codes employing the so-called Volume of Fluid (VOF) technique to track the interface evolution. Yet the stiffness of the problem under the specific experimental conditions is so large (initial explosive bubble growth, extremely large Marangoni number) that it precludes the possibility of numerical solution at reasonable computation times.

A previous attempt to simulate the problem was based on a

spherically symmetric (1-D) model for the liquid around a bubble that grows at a uniform and constant (time independent) internal temperature chosen within the range of values attained by the heating thermistor after nucleation. The far field temperature was set equal to the initial bulk liquid temperature.[23] The problem was solved using a well-known similarity transformation[24,25] and has led to a power law relation between bubble radius and time with an exponent value equal to 0.5, which gave predictions close to the measured data for short bubble growth times (up to 1-2 s). For larger times, the experimental curves were best-fitted by lower (than 0.5) exponent values, which meant that the bubble temperature should be decreasing with time. Part of this temperature decrease was attributed to the measured small temperature decrease of the thermistor itself during bubble growth, which, however, was not large enough to match up with the predicted low bubble temperature. The possibility that the discrepancy was due to the temperature dependent physical properties of the liquid or a radial temperature distribution inside the bubble was dealt with in another publication,[26] which showed that those could not be the major reasons for the discrepancy.

Keeping in mind that the driving force for bubble growth is the difference between the dissolved gas bulk concentration and the equilibrium concentration (solubility) at the bubble surface temperature, one can go a step further. The problem can be approximated again by a 1-D model for the liquid under the assumption, though, that the bubble grows at a uniform but time dependent temperature. This temperature is the instantaneous average temperature across the whole bubble. It must be noted that the volumetric and surface average temperatures of the bubble coincide, since the intra-bubble temperature field is dictated by the heat conduction (Laplace) equation.

Evidently, the computation of the evolution of the instantaneous average bubble temperature requires knowledge of the complete temperature field, which is not known. So, based on the simplified 1-D model, an inverse problem can be formulated. This calls for estimating the average bubble temperature evolution curve, $T_b(t)$, from the experimental bubble growth curve. Comparing the estimated average bubble temperature evolution with the measured temperature of the heating thermistor reveals important information for the phenomena dictating bubble growth. It must be noted here that the inverse problem does not involve the energy balance on the bubble surface (including terms such as latent heat, heat capacity of gas/vapor, heat of gas dissolution, gas expansion work, and so forth) since the bubble temperature is deduced from heat and mass transfer considerations on the liquid side combined with the bubble growth curve.

Formulation of the 1-D simplified problem

Let's consider a bubble with a temperature evolution, $T_b(t)$, growing in a liquid saturated with dissolved gas at a far field constant temperature T_o. Due to the relatively slow bubble growth (growth rates smaller than 1 mm/s), the Rayleigh Plesset equation degenerates to the expression[26]

$$P_v + P_g = P_\infty \tag{1}$$

where P_∞ is the ambient pressure and P_v, P_g the partial pressure of vapor and gas in the bubble, respectively. The terms that contain time derivatives of the bubble radius, R, in the Rayleigh-Plesset equation can be neglected due to the slow growth of the bubble. These terms are important in boiling applications where typical growth rates are of the order of mm/μs. Furthermore, the contribution of surface tension (Laplace pressure) to bubble evolution has been studied in detail by Cable and Frade.[24] According to these authors, the effect of surface tension is important for bubbles smaller than 50 μm but as they grow further, this effect gets less and less. So, for the present work where the model is used to infer temperatures of bubbles larger than 50 μm, the effect of surface tension can be ignored.

The dissolved gas concentration field is given from the solution of the following transient convection-diffusion equation:

$$\frac{\partial c}{\partial t} = \frac{1}{r^2}\frac{\partial}{\partial r}\left[r^2 D(T)\frac{\partial c}{\partial r}\right] - \dot{R}\frac{R^2}{r^2}\frac{\partial c}{\partial r} \qquad \text{for } R < r < \infty \tag{2}$$

It is very important to take into account the temperature dependence of diffusivity since it is very large (more than 250% increase of diffusivity between 40°C and 90°C for the system CO_2/water). Similarly, a significant variation with temperature exists for the solubility of CO_2 in liquids. Diffusivity and solubility data for the systems CO_2/water and CO_2/n-heptane are displayed in Figure 1a. Accordingly, Figure 1b presents vapor pressure versus temperature data for water and n-heptane.

For a negligible mass fraction of the solute gas in the liquid phase,[27] the mass balance of the gas in the bubble reads

$$\frac{d}{dt}\left(\frac{4}{3}\pi R^3 \rho_g\right) = 4\pi R^2 D(T_b)\left(\frac{\partial c}{\partial r}\right)_{r=R} \tag{3}$$

The gas molar density is related to the bubble temperature through the ideal gas law:

$$\rho_g = \frac{P_g}{R_g T_b} \tag{4}$$

The variation of the gas density is, in general, very small with respect to the variation of R^3, which varies by many orders of magnitude, so it can be placed out of the time derivative in the left-hand side of Eq. 3.

The boundary condition for the concentration on the moving boundary r = R(t) is

$$c(R, t) = c_{sat}(T_b) \tag{5}$$

where $c_{sat}(T)$ is the solubility of the gas in the liquid at temperature T and pressure P_∞ (total pressure) or, equivalently, at partial pressure of gas P_g.[28] Finally, the temperature dependence of the solvent vapor pressure is needed to close the problem.

$$P_v = P_{sat}(T_b) \tag{6}$$

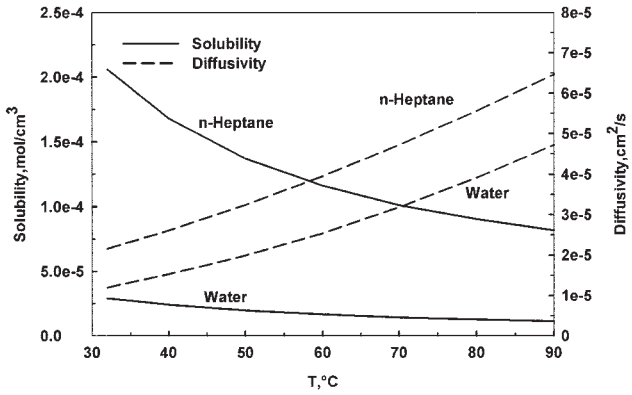

(a)

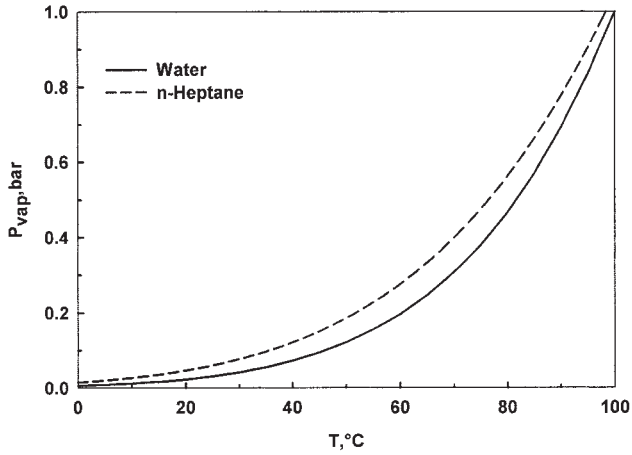

(b)

Figure 1. (a) Diffusivity and solubility data for the systems CO_2/water and CO_2/n-heptane; (b) Vapor pressure vs. temperature data for water and n-heptane.

The initial and the far field boundary condition for the concentration are

$$c(r, 0) = c(\infty, t) = c_o = c_{sat}(T_o) \tag{7}$$

and it is assumed that the bubble grows from a zero initial size (that is, R(0) = 0).

In addition to the above, the temperature profile in the liquid is needed for the computation of D(T) in Eq. 2. For the growth rate under consideration (smaller than 1 mm/s), conduction dominates the heat transfer process and the following quasi-steady temperature profile can be assumed:

$$T(r, t) = T_o + \frac{R(t)(T_b(t) - T_o)}{r} \tag{8}$$

Such a simplification is not generally valid for the concentration equation since the mass diffusivity, D, is much smaller than the thermal diffusivity of water.

Approximate solution of the problem

The above problem includes a transient convection-diffusion equation in semi-infinite domain with a moving boundary, so its numerical solution is by far non-trivial. Special techniques based on moving (Lagrangian) grids with careful discretization have been developed in the literature for the particular problem of bubble growth.[2] The use of the complete numerical solution of the direct problem makes the inverse problem quite difficult since repeated solutions of the direct problem are needed to determine the required temperature evolution (still without any guarantee for convergence). Here an approximate solution of the direct problem is derived that makes the inverse problem straightforward.

The main dimensionless parameter of the bubble growth problem is the so-called Foaming number (see Lastochkin and Favelukis[25] and references therein), which for the present case is time dependent (through the time dependency of T_b) and is given as

$$F_m = \frac{(c_{sat}(T_o) - c_{sat}(T_b))\, R_g T_b}{P_\infty - P_{sat}(T_b)} \tag{9}$$

This number denotes the ratio of the relative contributions of convection over diffusion phenomena of CO_2 from the bulk to the bubble surface. Diffusivity does not appear explicitly in the equation since convection is also proportional to diffusivity so it is eliminated and only driving forces eventually show up in the ratio.

Assuming that the gas molar density ρ_g can be moved out from the parenthesis in Eq. 3, an approximate solution exists for the problem in the limits $F_m(t) \ll 1$ and $F_m(t) \gg 1$.

Case $F_m \ll 1$

In this case the concentration field can be considered quasi steady (similar to the temperature flow field) and the bubble growth rate can be found as

$$\frac{dR}{dt} = \frac{1}{R} F_m D\left(\frac{T_o + T_b}{2}\right) \tag{10}$$

Case $F_m \gg 1$

In this case, the thickness of the concentration boundary layer is very small in comparison to the bubble radius, so the bubble curvature can be ignored. Plesset and Zwick[29] solved analytically the problem for constant F_m in this limit and found the following equation for the bubble growth rate:

$$\frac{dR}{dt} = \frac{1}{R}\frac{6}{\pi} F_m^2 D(T_b) \tag{11}$$

An integral solution method using polynomial trial functions has been proposed for the limit $F_m \gg 1$ by Rosner and Epstein[21] and has been used widely by several authors.[2,4] This method can be applied to time dependent F_m (present case) and gives:

$$\frac{dR}{dt} = \frac{1}{R} z F_m^2 D(T_b) \tag{12}$$

where the coefficient z takes the value 3 and 3.333 for polynomials of second and third order, respectively. It is noted that Eqs. 11 and 12 are of similar form and differ in just a numerical constant. In order to be compatible with the exact solution in the case of constant bubble temperature, we assume henceforth that $z = 6/\pi$.

It should be noticed here that, for $F_m \ll 1$, the concentration and temperature fields are of the same extent, so the diffusivity appearing in Eq. 10 is computed at the average field temperature. On the contrary, for $F_m \gg 1$, the concentration field is much thinner than the temperature field and the diffusivity in Eq. 11 is computed at the bubble temperature.

To take a composite relation for the bubble growth rate valid for all values of F_m, the two asymptotic rates are combined using a generalized interpolation scheme:

$$R\frac{dR}{dt} = \left(\left[F_m D\left(\frac{T_o + T_b}{2} \right) \right]^{-f} + \left[\frac{6}{\pi} F_m^2 D(T_b) \right]^{-f} \right)^{-1/f} \tag{13}$$

The solution of the above equation for a zero initial bubble size is given simply as:

$$R^2 = \int_0^t \left(\left[2F_m D\left(\frac{T_o + T_b}{2} \right) \right]^{-f} + \left[\frac{12}{\pi} F_m^2 D(T_b) \right]^{-f} \right)^{-1/f} d\tau \tag{14}$$

The exponent f is chosen based on the requirement for closest approach between the approximate and exact solutions in the case of constant temperature T_b and constant diffusivity. In this case, the following well-known analytical solution exists[18]:

$$R^2 = 4\beta^2 t \tag{15}$$

where β is given from $\varphi(\beta) = F_m$ with

$$\varphi(z) = 2z^2 \int_0^1 \exp[-z^2((1-y)^{-2} - 2y - 1)]dy \tag{16}$$

It is found that the exponent $f = 0.8$ yields a close proximity between the exact and approximate values of β, especially for $0.1 < F_m < 10$, which is the region of main practical interest. The comparison between exact and approximate values of $4\beta^2$ for $f = 0.8$ is shown in Figure 2.

Solution of the inverse problem

The above approximate solution of the bubble growth problem can be trivially inverted to give the bubble temperature evolution corresponding to an experimentally measured bubble growth curve, R(t). At each time moment the quantity $(dR^2/dt)_{exp}$ is computed from the experimental curves, and the corresponding values of the bubble temperature T_b is found by solving (using the Newton-Raphson method) the following non-linear algebraic equation:

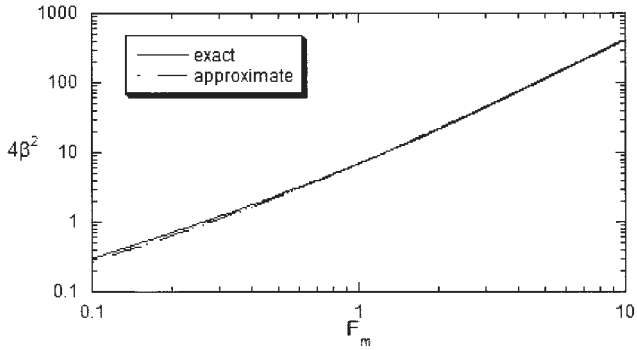

Figure 2. Comparison between exact and approximate values of $4\beta^2$ for f = 0.8.

$$\left(\left[2F_m D\left(\frac{T_o + T_b}{2} \right) \right]^{-0.8} + \left[\frac{12}{\pi} F_m^2 D(T_b) \right]^{-0.8} \right)^{-1.25} = \left(\frac{dR^2}{dt} \right)_{exp} \tag{17}$$

The time derivatives $(dR^2/dt)_{exp}$ are computed by fitting low order polynomials to the R^2 curves and differentiating analytically. This procedure is crucial to get rid of the high frequency noise in the measurements.

Experimental

Experimental setup

The experimental setup was described in detail by Divinis et al. [23] Here the major components are presented briefly, with emphasis to key improvements compared to that earlier work.

The core of the equipment is a thermostat unit, a CPF-2 type, into which an exchangeable sample cell unit is inserted (Figure 3). The thermostat operates under the gradient reduction principle and can provide precise temperature stability in the order of ± 0.005°C. In addition, the thermostat is equipped with optical and electronic interfaces that enable the stimulation and observation of the test fluid.

A sample cell unit is essentially a sealed tube, the lower part of which is made of special spectrometer glass cuvette with an internal diameter of 1.5 cm. The cells are specially designed to maintain their measuring chamber (glass cuvette) completely full with liquid in all times so as to prevent free float of the liquid in microgravity. The liquid volume in the cell is approximately 22 cm^3. The pressure inside the cells is kept at ambient values by means of an elastic membrane sealing a port of the cell. Two types of heaters are accommodated inside the test cells, placed apart by 5.5 cm in the longitudinal direction: a small axisymmetrical NTC thermistor (Thermometrics, Inc. $r_{th} = 0.125$ mm, nominal, time constant in water = 0.01 s) to serve as a local roughly spherical heater, and a flat platinum resistance layer (3×7 mm, approximately 1 mm thick) deposited on a special non-conducting support to serve as a flat surface heater. Here results only from the former will be presented.

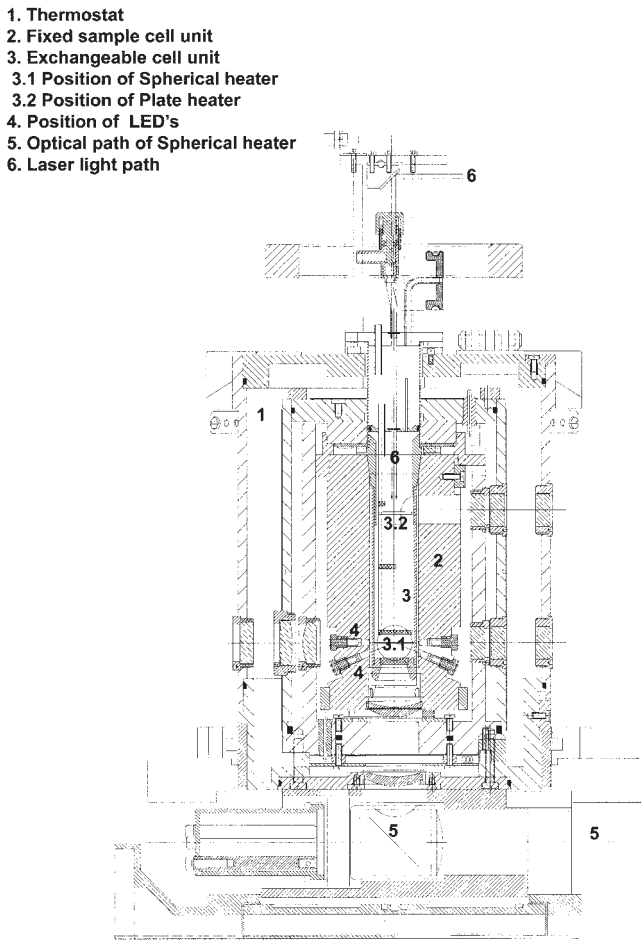

Figure 3. Thermostat unit with an exchangeable cell.

The bubbles growing on the spherical heater are illuminated from the side by RGB light emitting diodes (LEDs). A similar side illumination technique has been recently used by Dehaeck et al.,[30] where bubble edge is identified by a proper analysis of the refracted and reflected light beams coming from the bubble surface. A 5 mW He-Ne Laser is used for background illumination to create strong contrast between the bubble and its surroundings (an improvement of this work that increased the accuracy of bubble size determination). Bubble images are recorded by a CCD color camera with 1k $\times$ 1k pixels, 24-bit resolution RGB and acquisition rate of 25 frames per second. This configuration allowed a spatial resolution around 10 μm, depending on the employed magnification factor of each run. Constant-power ($\pm$2%) heating pulses are applied to the heating thermistor through a special circuitry. Registering the voltage drop across the heater with a sampling frequency of 10 Hz allows the delivered power and temperature of the heater to be calculated. A thermistor (same size as the heating thermistor) measures the bulk liquid temperature at a distance 2.5 mm in the longitudinal direction away from the heater surface. The thermal performance of the equipment is supervised by a custom-made software.

De-ionized water, n-heptane (99.0%, Panreac quimica), and a mixture of glycerin-water 42–58% w/w (>99.5% glycerol, BDH Laboratories supplied) are the test liquids examined in this study. All test liquids are initially saturated with CO_2 (99.99%, air metal), a gas chosen mainly because of its practical significance and its large solubility in liquids, which gives easy birth to the phenomena we wish to investigate.

Experimental procedures

The experiments were performed during the 35th and 38th ESA's Parabolic Flight Campaigns. On the whole, 57 runs have been successfully performed with the small axisymmetrical heater producing single bubbles (including the repeatability runs). Several other runs (not reported here) involve multiple bubble generation on the thermistor or use of a flat plate heater. Each run is conducted during a separate parabola, which provides a sequence of normal-high-low-high-normal gravity phases. The gravity value during the low gravity phases fluctuates randomly within $\pm 2.6 \times 10^{-2}$ g, whereas during the high gravity phases it reaches a peak value of about 1.6–1.8 g. The low gravity period is slightly different among parabolas but on the average lasts approximately 20 seconds.

The saturation of the test liquids with CO_2 is conducted on the ground just before the flight. This is realized by bubbling the liquids with the gas at 32°C (this is the bulk liquid temperature for all runs), using improved thermal control devices (compared with the previous work), for about 60 min. This time lapse is chosen based on wet analysis of water samples exposed to CO_2 bubbling for varying time intervals.[31] Next, the saturated liquids are used to fill 10 sample cell units, carefully purged and flooded with CO_2. A thermally regulated storage cabinet, part of the flight apparatus, is used to maintain the test cells at a temperature 2°C below the saturation temperature.

Two types of experiment are examined here. The first one refers to single bubbles growing at the bare tip of the small thermistor by employing continuous heat pulses. The power of the pulses is constant through each run but varies among runs. A brief outline of the experimental scenario is as follows. An exchangeable test cell is inserted in the thermostat and is left to equilibrate at a temperature a few tenths of a degree below the liquid's saturation temperature. Then the temperature of the liquid is raised locally by energizing the heater at a preset power level and for a 10 s duration. This is done about 7 s after the onset of the low gravity phase during a parabola to ensure that the experiment would indeed start at good low gravity conditions. After the onset of heating, a short time period is necessary to create local superheat and therefore cause nucleation, whereafter a bubble forms and grows on the thermistor's surface. After five consecutive parabolas, the test cell is exchanged with a new one.

The second type of experiments examined here refers to intermittent growth of single bubbles at the small thermistor by applying two short heat pulses separated by a small inert time

Table 1. Range of the Delivered Power Levels for the Different Test Liquids that Produced Single Bubbles

Liquid	Power Range, mW	Heat Flux Range, W/m^2	$T_{ave.}$ Range*, °C
Water	66.0–11.0	8.0×10^4–1.3×10^4	87.0–51.0
n-Heptane	25.0–6.0	3.9×10^4–0.9×10^4	58.0–33.0
Glycerin-water mixture	77.0–48.0	11.0×10^4–6.8×10^4	110.0–98.0

*$T_{ave} = (T_{max} + T_{min})/2$.

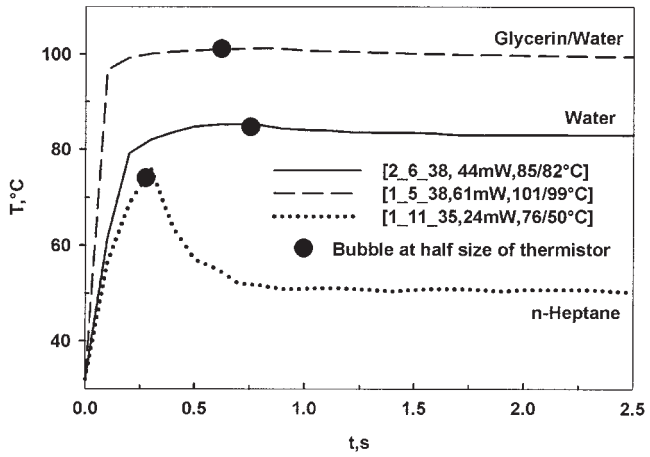

Figure 4. Typical patterns of the thermistor data during experimental runs with the three test liquids for the first instances of bubble growth (2.5 s).

interval. The power levels of the two short pulses are equal to each other and in a range of values similar to the continuous pulses. As in the continuous single bubble growth experiments, about 7 s after the onset of the low gravity phase during a parabola, a short heat pulse (~1.5–2 s) is given such as to produce a bubble roughly at the size of the thermistor. This is followed by an approximately 5 s inert period and, after that, a heat pulse of the same power is given for another 10 s.

Table 1 displays the range of the delivered power levels for the different test liquids that produced single bubbles. The corresponding average thermistor temperatures and estimated heat fluxes—assuming that the heater is perfectly spherical—are also presented. The present work complements the data of Divinis et al[23] by employing broader heating power ranges, especially towards lower values where preferably single bubbles are produced.

An enhanced image processing code written in MATLAB® was used to determine the bubble diameter from video frames. This software improvement combined with the increased contrast due to the laser back-lit of the bubble leads to bubble radius values different by at most 8% from those reported by Divinis et al.[23] The overall uncertainty in the measured bubble radius is ±2%. The known speed of the camera allows determination of bubble radius as a function of time. "Zero" time is designated to be the last vacant frame before a bubble appears on the digital tape and is used to estimate the initial nucleation time delay between onset of a heat pulse and bubble appearance. It must be stressed here that due to the employed spatial and temporal resolution in video recording, it is not actually possible to follow bubble growth right from the moment of nucleation, but these size (~1 μm) and time (~1 μs) regimes are beyond the interests of this work.

Results and Discussion

Thermal data

Among the most important data for the interpretation of the experiment is the temperature history of the heating thermistor. On the contrary, the temperature of the bulk, measured by a thermistor located 2.5 mm in the longitudinal direction away from the heater, is not influenced by the local heating, as manifested by recorded increases of less than 0.2°C during heat pulses.

Figure 4 displays typical patterns of the thermistor data during experimental runs with the three test liquids for the first instances of bubble growth (2.5 s). Initially, the thermistor temperature rises very fast because of its low heat capacity value. Its thermalization speed increases considerably with the applied power. The relative size of the developing bubble with respect to the size of the thermistor determines the thermal response of the thermistor. When the bubble is relatively small, the thermistor temperature continues to climb fast (perhaps not as fast as before nucleation, but there is not enough time resolution in temperature readings to assert this). The moment the bubble reaches a critical size (roughly equal to half the size of the thermistor), the thermistor stops getting warmer and even starts to cool down since the growing bubble absorbs from it a progressively increasing amount of heat. Two different trends of the thermistor temperature are observed among test liquids when a bubble reaches roughly half the size of the thermistor. One trend, observed in water and in the glycerin-water mixture, involves a slow decay after a peak value. This is in contrast to the immediate rapid decay observed in n-heptane. The above difference may be attributed to the high growth rate of n-heptane bubbles compared with the other two liquids.

Nucleation of a single bubble occurs exclusively at a specific preferred site on each thermistor (heterogeneous nucleation). Such a preferential nucleation is usually ascribed to vapor/gas trapped in submicroscopic imperfections on the thermistor's surface.[15] With respect to nucleation, it is noted that—unlike the typical temperature profile presented in Figure 4—there are experimental runs where appreciable time is needed for nucleation to occur. On this account, Figure 5a compares bubble radius evolution and thermistor temperature curves for a particular run in water where the nucleation time delay in initial bubble formation is marked. This time lag can be clearly identified also in the thermistor temperature data, which show a steep increase before bubble nucleation. The same heater behavior is registered by Lee et al.[32] in performing pool boiling experiments with R-123. Two limiting temperature values (T_{max} and T_{min}) are noted in the plot designating the temperature range within which the bubble grows. (The [x x x,x,x/x] format in the legend stands for [day parabola campaign, power, T_{max}/T_{min}]).

Figure 5b displays a relationship between the time of nucleation time delay and the time-weighted average thermistor readings after the formation of the bubble. The respective power values for each run are included in the plot. What is noted for all the fluids used is that nucleation time delay decreases promptly as the temperature of the heater increases. A similar observation has also been made by Merte and Lee.[32]

Nucleation time delay may be understood in terms of the time taken by a liquid to attain the degree of supersaturation necessary for nucleation of bubbles. The ranges of nucleation time delay values observed are 0.64–3.5 s for glycerin-water solution, 0.08–0.3 s for n-heptane, and 0.24–1.4 s for water. The supersaturation values, σ, corresponding to the temperature of bubble nucleation, T_n, are calculated, according to the definition $\sigma = (C_{sat}(T_0)/C_{sat}(T_n)) - 1$ and the results are $\sigma = 0.8$–1.2 for water, $\sigma = 0.9$ for glycerin-water solution, and

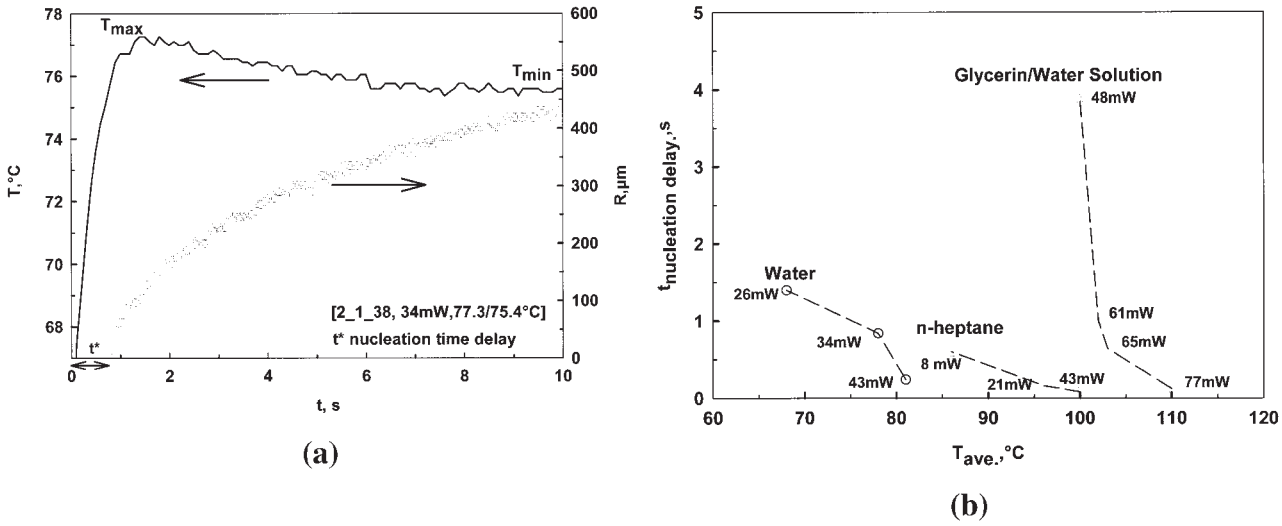

Figure 5. (a) Comparison of bubble radius evolution and thermistor temperature curves for a particular run in water where the associated nucleation time delay in initial bubble formation is marked; (b) relationship between the nucleation time delay and the time weighted average temperature readings of the corresponding experiments where nucleation time delay is observed.

σ = 0.1–0.3 for n-heptane. There is an order-of-magnitude agreement between the present data and the observation by Jones et al.,[14] who showed that bubbles in carbonated water are produced at levels of supersaturation below a value of two.

Figure 6 shows the applied heating powers and ensuing thermistor temperatures covered by this work and also by the work of Divinis et al.,[23] and indicates the progress achieved by the present contribution. Clearly, the present work is an extension of that earlier study towards lower power levels since higher powers were always leading to simultaneous generation of multiple bubbles. For clarity only, maximum temperatures are shown. Two points are noted with respect to Figure 6. First, there exists an approximately linear relation between thermistor power and temperature. The inclination angle is different for each liquid, and—as expected—is directly related to the liquid's thermal conductivity (Figure 1a). Second, different power levels (thus, temperatures) are necessary to generate single bubbles in the two liquids. This is inversely related to the gas solubility in the two liquids (Figure 1b).

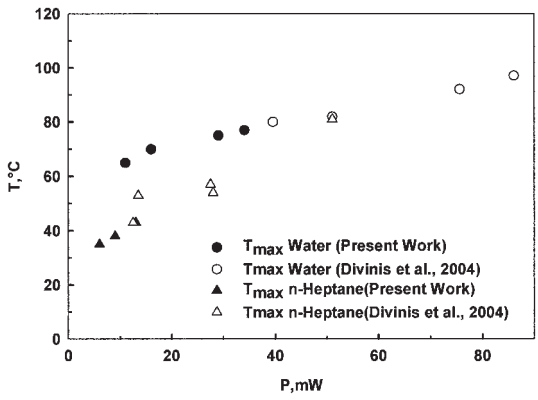

Figure 6. Applied heating powers and attained thermistor temperatures covered by this work and also by the work of Divinis et al.[23]

Bubble growth data

The growth rate of single bubbles (independent of the liquid used) depends strongly on the power delivered by the thermistor and its corresponding temperature. Figure 7a,b,c documents this behavior (for water, water-glycerol, and n-heptane, respectively) by displaying the temporal variation of bubble radius for various input powers. For completeness, some data from Divinis et al.[24] are also included. In all the figures, time "zero" corresponds to the visual appearance of the bubble and not to the onset of the heat pulse, so that comparisons are not hindered by differences in nucleation time delay. The power delivered to the thermistor and the corresponding temperatures are independent of the nucleation time delay. It is noted that repeatability of the above data is better than 3%.

The following characteristics of the experiment are noted: First, there exists a minimum temperature threshold, different for each liquid, below which no bubble appears. This limit is around 64°C for water, 97°C for water-glycerol, and 35°C for n-heptane. Second, a monotonic increase of the bubble growth rate with thermistor temperature is observed in all cases. Third, a gradual leveling off takes place at high thermistor powers, with the result that further increase in power produces insignificant rise of the bubble growth curve (more about this later). These limiting curves are included in all Figures 7a,b,c, and a convincing demonstration is provided by Figure 7c (n-heptane), where the upper two growth curves almost coincide although the corresponding thermistor temperatures differ by around 20°C.

Another persistent feature in most of these curves is that the temperature of the thermistor is not constant during bubble growth but varies between a maximum value (shortly after bubble inception) and a minimum value (usually at the end of

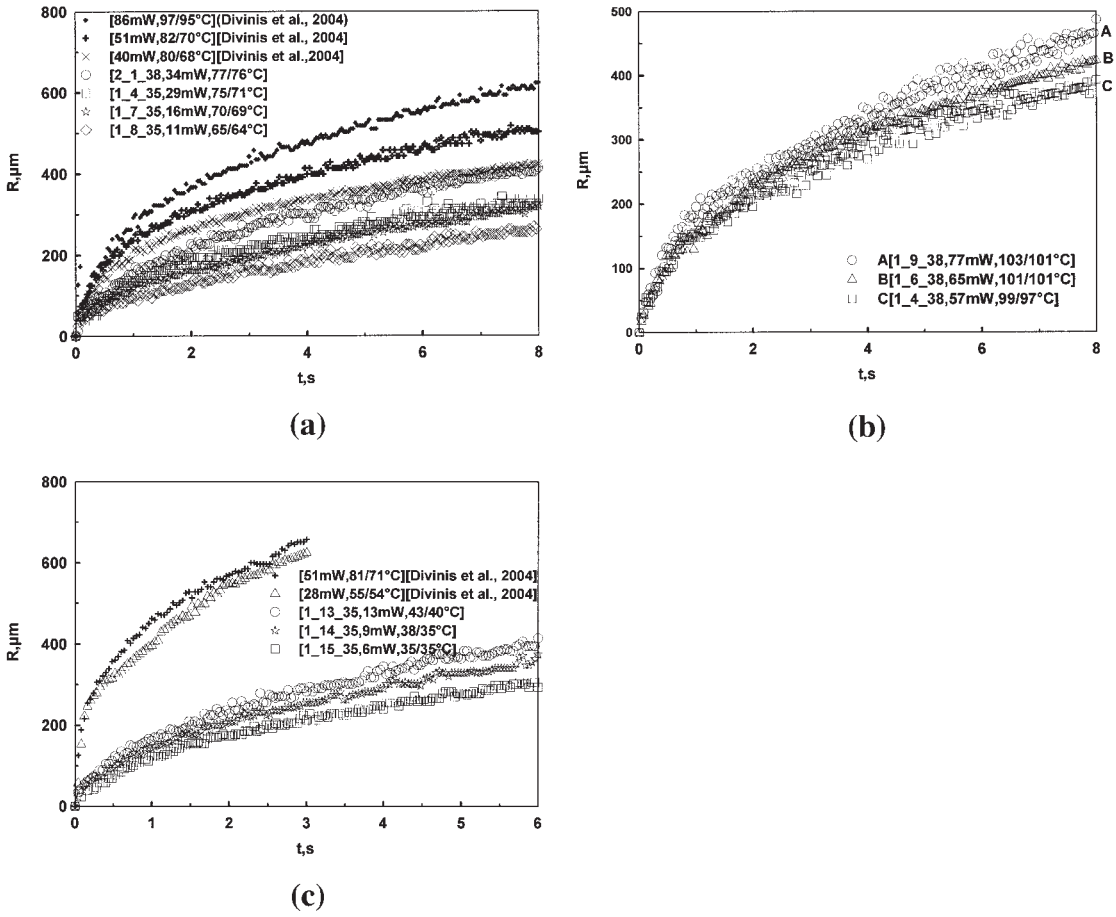

Figure 7. Single bubble growth data under different power and temperature of the heating thermistor.

(a) Water, (b) glycerin/water mixture, (c) n-Heptane.

the heating pulse when the bubble is largest). The extent of this variation seems to depend on both test liquid and heating power. Thus, the bubble grows under non isothermal conditions, and the particular temperature profile developing in each run, as will be shown later, plays a decisive role in the growth rate.

Figure 8 compares single bubble growth data for the three test liquids. If one takes into account the respective power

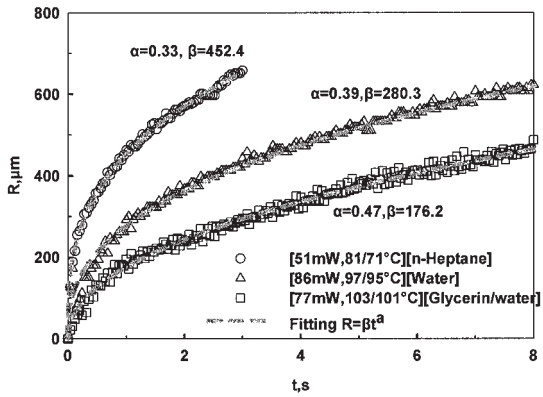

Figure 8. Comparison of single bubble growth data for the three test liquids.

levels and temperatures of the thermistor for each run, it is clear that the fastest growth is observed in n-heptane, whereas the slowest growth is in glycerin-water mixtures. The shape of the growth curves can be described with a power law ($R = \beta t^{\sim\alpha}$), with different values of the exponent α. As can be seen, heptane (with the highest growth rate) exhibits the greatest deviation from $\alpha = 0.5$, followed by water (intermediate growth rate) and water-glycerin (lowest growth rate). In other words, the test fluid physical and transport properties chiefly dictate the growth pattern.

Figure 9a presents fitted values of α against the maximum thermistor temperature for all test fluids. For a specific test fluid, the divergence from 0.5 first increases drastically with increasing temperature (that is, higher growth rates) and then appears to approach asymptotically a constant value. Furthermore, the dependence of β on the maximum thermistor temperature, Figure 9b, supports the arguments made in Figure 7 that the growth rate does not infinitely increase but as the temperature increases it eventually levels-off at a maximum (plateau) value. This value is different for each liquid.

Intermittent bubble growth experiments have also been undertaken with the application of two short heat pulses separated by an idle time interval. In this way, bubbles reach initially a desired small size (usually close to the size of the thermistor), and then the second heat pulse triggers their further growth.

Figure 10a displays two indicative curves of such runs in water. In the 1st growth period (GP), the bubble reaches approximately the thermistor size. The heating time to do so depends on the power level selected. The 1st GP is followed by a waiting period, where the bubble starts to shrink chiefly due to gas re-dissolution and also some vapor condensation. The degree of shrinkage during the waiting period in the present experiments is proportional to the delivered power. Thus, run A of Figure 10a shows a shrinkage rate of 1.5% per second (5 s waiting time); whereas run B, with 40% higher power level, shows a shrinkage rate of 3% per second (7 s waiting time).

The final growth (2nd GP) of the pre-existing bubbles is accomplished by a second heat pulse of the same intensity as the first. The resulting composite bubble evolution is shown for the two experiments, A and B, in Figure 10b, where the waiting period is not included and the final growth curves are moved to the left. It is interesting to observe that the two experiments reach the same final bubble size despite the difference in thermistor power. This intuitively unexpected result is attributed to the shrinkage effect of the waiting period, which is stronger for the higher power.

Next, it is attempted to interpret the present data in terms of the developed model of one-dimensional bubble growth with

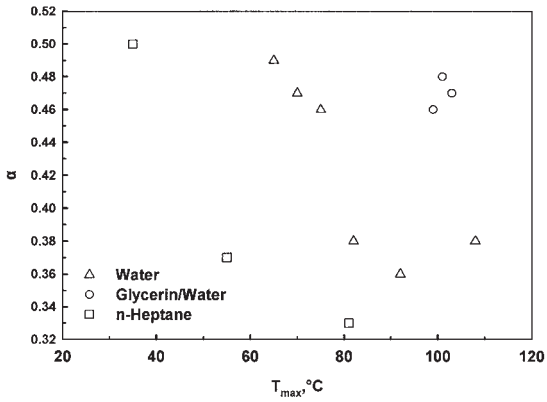

(a)

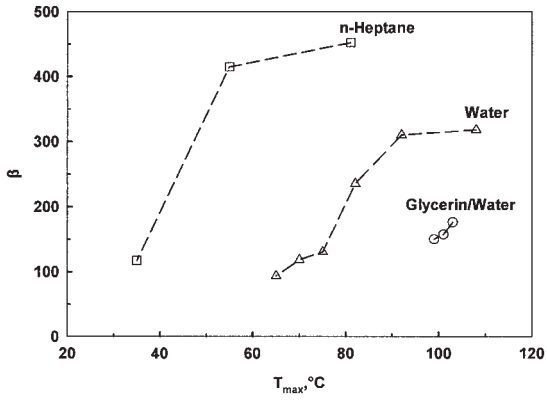

(b)

Figure 9. (a) Computed values of α against the maximum thermistor temperature for all test fluids; (b) computed values of β against the maximum thermistor temperature for all test fluids.

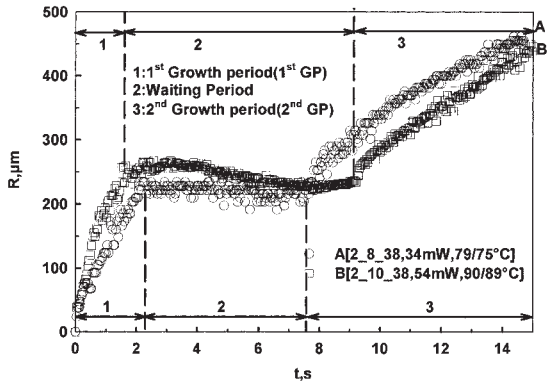

(a)

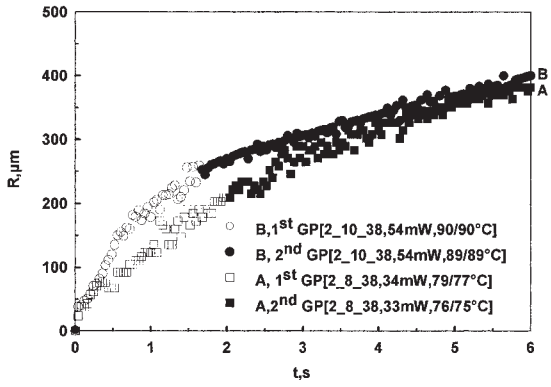

(b)

Figure 10. (a) Two indicative curves of intermittent bubble growth experiments; (b) resulting composite bubble evolution for the two experiments.

time-dependent bubble temperature. More specifically, the model is used to transform experimentally determined bubble radius evolution curves into average bubble temperature evolution curves. Figure 11 displays representative bubble growth curves for each liquid tested and the best fit by a third order polynomial ($R^2 > 0.98$) used in the computation. In attempting to use differential methods for data analysis, problems are frequently encountered with slight scatter of the data, which could bring about large changes in the goodness of the fit. Due to the employed moderate temporal and spatial resolution in recording bubble growth, such problems occur here for images of small, fast growing bubbles, that is, right after the onset of heating. As a result, at such short times the model cannot yield an accurate determination of average bubble temperature from the slopes between consecutive bubble radius data and, therefore, the aforementioned transformation is applied only to larger bubble radii (a few tenths of a second after nucleation).

The average bubble temperature computed from the model is compared in Figure 12 to the measured thermistor temperature. Figure 12a displays results for water at two different heating powers (A and B) and indicates that bubble growth is isothermal with the thermistor for a time period ranging around 1–4 s. This is rather expected since at such short times, the bubble is still small and pretty close to the thermistor. After that time,

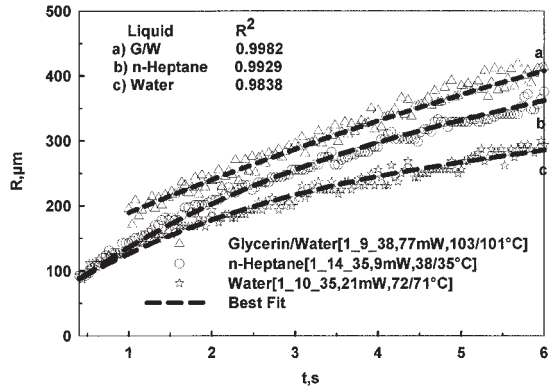

Figure 11. Representative bubble growth curves for each liquid tested and the best fit by a third order polynomial used in the computation.

there is a growing deviation of the order of a few degrees between the temperatures of the thermistor and those predicted by the model. As the power provided by the thermistor increases, the time the bubble remains isothermal decreases, and the deviation from the thermistor temperature towards the end of the thermal heat pulse becomes greater (experiment A).

Figure 12b shows the same comparison as above, only now for two different runs with the water-glycerol system. Here, it is observed that the predicted mean bubble temperature coincides with the measured thermistor temperature for most of the duration of the heat pulse (experiments A and B). The agreement is attributed to the slow growth of bubbles in water-glycerol, which provides enough time for the thermistor to equilibrate thermally with the bubble. Figure 12c refers to the n-heptane system. Here, bubbles growing at small superheat are in thermal equilibrium with the thermistor (experiment B), but higher heater temperatures result in very strong deviations between thermistor and mean bubble temperatures (experiment A).

The mechanistic picture emerging from the above results is that, during its growth, a bubble extends into progressively colder liquid. Thus, its average temperature falls below that of the heater and of the liquid in the heater's immediate vicinity. Evidently, the deviation between bubble and thermistor temperature is expected to become more significant the faster the growth and the larger the size of the bubble. This also explains qualitatively the observed saturation of the growth rate with increasing thermistor power. Finally, it must be noted that the inevitable thermocapillary (Marangoni) convection around the non-isothermal bubbles (incorporated in the experimental growth curves) acts to reduce the deviation between average bubble temperature and thermistor temperature. Marangoni convection is a complementary physical mechanism, driving

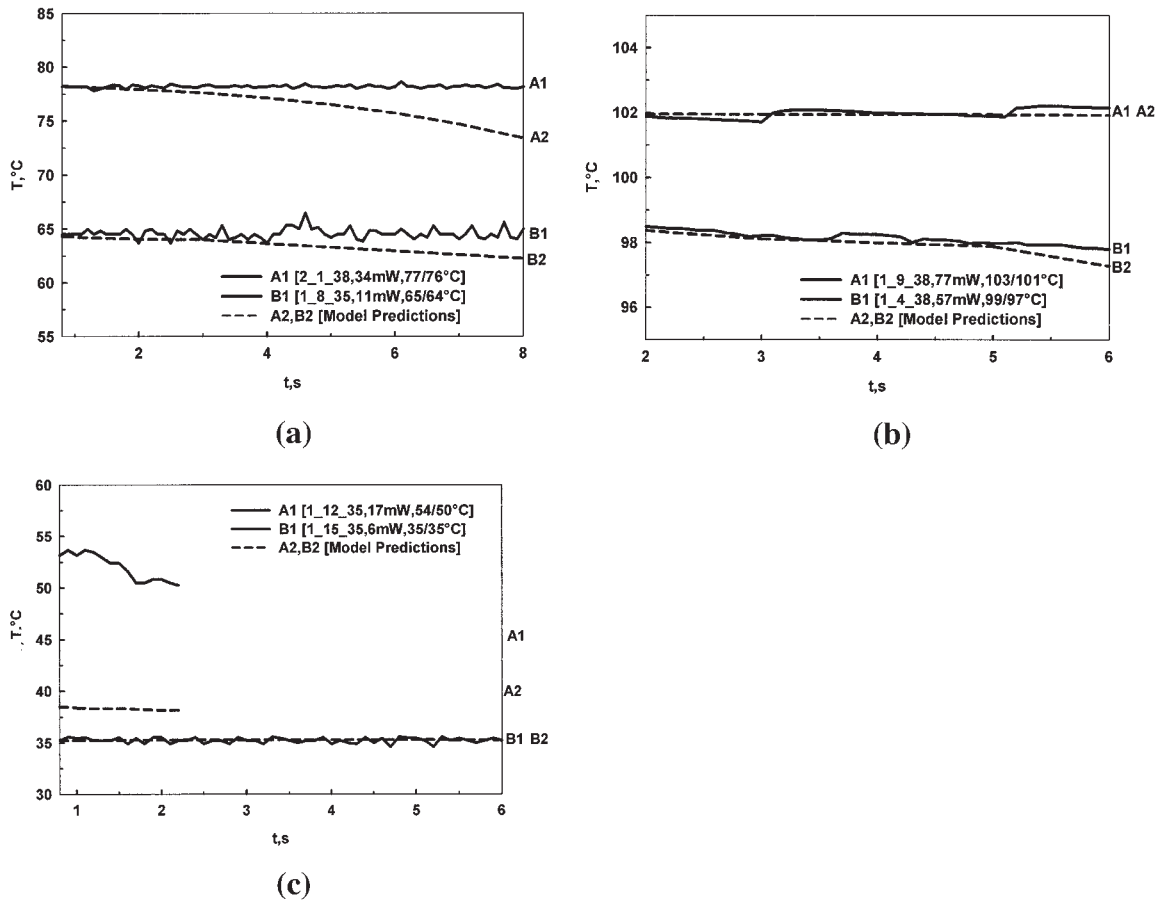

Figure 12. Average bubble temperature computed from the model compared to the measured thermistor temperature.

a) Water, (b) gycerin/Water mixture, (c) n-Heptane.

liquid from the warm base of a bubble towards its cold apex, mitigating temperature gradients around the bubble, and thus contributing to the establishment of thermal equilibration between thermistor and bubble.

Conclusions

For each test fluid, there is a clear relation between bubble nucleation time delay and temperature of the miniature thermistor (acting as the local heater). Moreover, the thermistor temperature varies linearly with the power of the applied heat pulses. As this temperature (or power) increases, the nucleation time delay decreases.

It is chiefly the physical and transport properties of the test fluids (gas solubility, mass diffusivity, and vapor pressure) followed afar by the power delivered by the thermistor that govern the rate of bubble growth by dictating the temperature and concentration profiles around the bubble. The bubble growth rates measured in n-heptane are much higher than those measured in water and glycerin-water solutions despite the fact that the delivered powers and heater temperatures for n-heptane are the lowest of all. For all liquids, increasing the power or, equivalently, the thermistor temperature leads to higher growth rates and stronger deviation from the $a = 0.5$ power law.

The model developed to describe the non-isothermal bubble growth based on experimentally determined bubble radius evolution curves shows that there is an initial period where the bubble grows in thermal equilibration with the heating thermistor. This period depends on the fluid and on the delivered power. So, in water it ranges from 2–4 s whereas in glycerin-water solution it lasts for the entire heating period, that is, 10 s. In n-heptane, bubbles growing at small superheat are in thermal equilibrium with the thermistor over the whole heating period. However, at high superheats, the average bubble temperature is already from the beginning of the heat pulse much lower than the thermistor temperature.

Acknowledgments

We are thankful to ESA for kindly providing the parabolic flights (ESA MSN/GA/2003–51/JV). The support of Dr. Vladimir Pletser of ESA and the personnel of Novespace during the flights is gratefully acknowledged.

Literature Cited

1. Steiner H, Kobor A, Gebhard L. A wall heat transfer model for subcooled boiling flow. *Int J Heat Mass Transfer.* 2005;48:4161-4173.
2. Arefmanesh A, Advani SG, Michaelides EE. An accurate numerical solution for mass diffusion induced bubble growth in viscous liquids containing limited dissolved gas. *Int J Heat Mass Transfer.* 1992;35: 1711-1722.
3. Payvar P. Mass transfer controlled bubble growth during rapid decompression of a fluid. *Int J Heat Mass Transfer.* 1987;30:699-706.
4. Yoo HJ, Han CD. Oscillatory behavior of a gas bubble growing (or collapsing) in viscoelastic liquids. *Am Inst Chem Eng J.* 1982;28:1002-1009.
5. Uhlmann DR. "Glass processing in a microgravity environment." *Materials Processing in the Reduced Gravity Environment of Space*. G. E. Rindone, ed. New York: Elsevier; 1982;269-278.
6. Clift R, Grace JR, Weber ME. *Bubbles, Drops and Particles*. New York: Academic Press; 1978.
7. Evans WC. Lake Nyos, knowledge of the Fount and the cause of disaster. *Nature.* 1996;21:379.
8. Barker GS, Jefferson B, Judd SJ. The control of bubble size in carbonated beverages. *Chem Eng Sci.* 2002;57:565-573.
9. Srinivasan RS, Gerth WA, Powell MR. A mathematical model of diffusion limited gas bubble dynamics in tissue with varying diffusion region thickness. *Respiration Physiology.* 2000;123:153-164.
10. Kislyakov YY, Kopyltsov AV. The rate of gas-bubble growth in tissue under decompression. Mathematical modeling. *Respiration Physiology.* 1988;71:299-306.
11. Van Liew HD, Burkard ME. Simulation of gas bubbles in hypobaric decompressions: roles of O_2, CO_2, and H_20. *Aviation, Space Environ Med.* 1995;66:50-55.
12. Li J, Peterson GP. Microscale heterogeneous boiling on smooth surfaces-from bubble nucleation to bubble dynamics. *Int J Heat Mass Transfer.* 2005;48:4316-4332.
13. Lee HS, Merte Jr H, Picker G, Straub J. Quasi-homogeneous boiling nucleation on a small spherical heater in microgravity. *Int J Heat Mass Transfer.* 2003;46:5087-5097.
14. Jones F, Evans GM, Galvin KP. The cycle of bubble production from a gas cavity in a supersaturated solution. *Adv Coll Interface Sci.* 1999;80:51-84.
15. Jones F, Evans GM, Galvin KP. Bubble nucleation from gas cavities—a review. *Adv Coll Interface Sci.* 1999;80:27-50.
16. Robinson AJ, Judd RL. Bubble growth in a uniform and spatially distributed temperature field. *Int J Heat Mass Transfer.* 2001;44:2699-2710.
17. Miyatake O, Tanaka I, Lior N. Bubble growth in superheated solutions with a non volatile solute. *Chem Eng Sci.* 1994;49:1301-1312.
18. Scriven LE. On the dynamics of phase growth. *Chem Eng Sci.* 1959; 10:1-13.
19. Saddy M, Jameson GJ. Experiments on the dynamics of phase growth. *Chem Eng Sci.* 1971;26:675-684.
20. Strenge PH, Orell A, Westwater JW. Microscopic study of bubble growth during nucleate boiling. *AIChE J.* 1961;7:578-583.
21. Rosner DE, Epstein M. Effects of interface kinetics, capillarity and solute diffusion on bubble growth rates in highly supersaturated liquids. *Chem Eng Sci.* 1972;27:69-88.
22. Bisperink CGJ, Prins A. Bubble growth in carbonated liquids. *Coll Surf A: Physicochemical Eng Aspects.* 1994;85:237-253.
23. Divinis N, Karapantsios TD, Kostoglou M, Panoutsos CS, Bontozoglou V, Michels AC, Sneep MC, de Bruijn R, Lotz HTh. Bubbles growing in supersaturated solutions at reduced gravity. *AIChE J.* 2004;50:2369-2382.
24. Cable M, Frade JR. Diffusion controlled mass transfer to or from spheres with concentration-dependent diffusivity. *Chem Eng Sci.* 1987;42:2525.
25. Lastochkin D, Favelukis M. Bubble growth in variable diffusion coefficient liquid. *Chem Eng Sci.* 1998;69:21.
26. Divinis N, Kostoglou M, Karapantsios TD, Bontozoglou V. Self-similar growth of a gas bubble induced by localized heating: The effect of temperature-dependent transport properties. *Chem Eng Sci.* 2005; 60:1673-1683,
27. Patel RD. Bubble growth in a viscous Newtonian liquid. *Chem Eng Sci.* 1980;35:2352-2355.
28. Fogg PGT, Gerrard W. *Solubility of Gases in Liquids: A Critical Evaluation of Gas Liquid Systems in Theory and Practice.* New York: Wiley Interscience; 1991.
29. Plesset MS, Zwick SA. The growth of vapor bubbles in superheated liquids. *J Appl Phys.* 1954;25:493-500.
30. Dehaeck S, van Beeck JPAJ, Riethmuller ML. Extended glare point velocimetry and sizing for bubbly flows. *Experiments in Fluids.* 2005; 39:407-419.
31. Bontozoglou V, Karabelas AJ. Direct-contact steam condensation with simultaneous noncondensable gas absorption. *AIChE J.* 1995;41:241-250.
32. Merte Jr. H, Lee HS. Quasi-homogeneous nucleation in microgravity at low heat flux: experiments and theory. *J Heat Transfer.* 1997;119: 305-312.

Manuscript received Feb. 27, 2006, and revision received Apr. 18, 2006.